Chapter 4. Experimental Characterization Optimising Alignment Parameters of GNP Epoxy Base nanocomposite

The contents of this chapter have appeared as:

A. Tiwari, S.K. Panda, S.K. Shaw, Experimental characterization optimizing the alignment parameter for GNP epoxy base nanocomposite via a weak DC magnetic field, ***Polymers for Advanced Technologies (2023)***. https://doi.org/10.1002/PAT.6137.

4.1. Introduction

In order to utilize the predictions of optimizing the influencing parameters for alignment in epoxy by the mathematical model, superparamagnetic magnetite nanoparticles (Fe_3O_4) were synthesized and applied to the surface of GNP. This process significantly increased the magnetic susceptibility of the decorated nanoparticles and enhanced their ability to respond to low-intensity external magnetic fields. The decorated nanoparticles were then dispersed in an epoxy matrix, and a weak DC magnetic field was applied to the mixture to produce aligned nanocomposites. The characterisation of GNP and Fe_3O_4-GNP and the degree of alignment in the nanocomposites were evaluated using various techniques such as X-ray diffraction (XRD), Fourier-transform infrared spectroscopy (FTIR), Raman spectroscopy, thermogravimetric analysis (TGA), Differential scanning calorimetry(DSC), atomic force microscopy (AFM), X-ray photoelectron spectroscopy (XPS), Brunauer-Emmett-Teller (BET) analysis, transmission electron microscopy (TEM), scanning electron microscopy (SEM), energy-dispersive X-ray microanalysis (EDXMA), and vibrating sample magnetometry (VSM)[162].

4.2. Experimental section

The consistency of the model being suggested is validated with experimental analysis and a completely cured nanocomposite with an aligned Fe_3O_4-GNP nanoparticles technique is developed. GNP has deficient magnetic capabilities to do this, so the surfaces of GNP are

functionalized with Fe_3O_4 and dispersed in small amounts in the epoxy. DC electromagnetic field is applied to the liquid epoxy with dispersed Fe_3O_4-GNP nanoparticles. Additionally, the orientation of the Fe_3O_4-GNP nanoparticles during curing is examined to verify the alignment report with the help of an optical microscope after a specific time interval. The characterization of cured nanocomposite and its alignment are critically analyzed and compared further through XRD, Raman, AFM, and SEM.

4.2.1. Basic materials

In this work, a most common thermosetting polymer for polymer composite, DGEBA based epoxy resin (LY-556) was used as matrix. As catalyst, hardener Aradur (HY-951) procured from Huntsman, Hyderabad was consumed as the curing agent. The matrix and curing agent's stoichiometric quantities were taken 10:1 by weight. The GNP used as nanoparticle reinforcement is obtained from XG Sciences, USA. The GNP comprises little piles of graphene sheets having a platelet shape. The particle diameter and thickness of the GNP are in the micron and nanometres range, respectively. The Fe_3O_4 nanoparticle was synthesized via solvo-thermal reaction and preparation of GNP epoxy and Fe_3O_4-GNP epoxy nanocomposites with complete characterizations of the nanoparticle along with nanocomposites[163].

4.2.2. Synthesis of Fe_3O_4 and Fe_3O_4-GNP

The Fe_3O_4 nanoparticle was synthesized via solvo-thermal reaction following the steps described elsewhere [164]. Briefly, $FeCl_3$ (anhydrous, CDH) (1.01 g) was added to 50 ml ethylene glycol (EG, CDH) and sonicated for 1 hour in a water-bath sonication system. Another solution containing sodium acetate (NaOAc, 3.6 g) dissolved in 20 ml EG was prepared with the help of sonication. This NaOAc solution was then added drop-wise to $FeCl_3$ solution and the mixture was stirred for 4 hours at 50-degree Celsius. Formation of brown precipitates was observed during this step. After stirring, the solution was then transferred to a 100 ml Teflon-lined autoclave which was placed in an oven at 200 °C for 24 hours. Finally, a black precipitate

was obtained, which was washed several times with double distilled (DD) water and finally with ethanol to remove organic solvent. The precipitate was dried overnight at 70 degrees. The final powder was characterized by following several techniques. For obtaining Fe_3O_4-GNP nanoparticles anhydrous $FeCl_3$ and GNP was added to 50 mL EG solution, rest process being same[163].

4.2.3. Preparation of GNP epoxy and Fe_3O_4-GNP epoxy nanocomposites

The Epoxy nanocomposites containing the highly dispersed nanoparticles were prepared by the procedure as outlined in **Fig. 4.1** . The GNP was mixed with Tetrahydrofuran (THF) (ratio 1-2 mg/ml), and the solution is mechanically stirred for 10 min. In the next step ultrasonic probe (7mm) sonicator is used to break the Vander wall forces between the nanoparticles for 40 min in an ice bath (cycle 0.5 seconds and 75% amplitude).

Epoxy is mixed with the above solution, and again, mechanical stirring for 10 min is carried out. The new solution is again sonicated for 40 minutes. To evaporate the solvent, magnetic stirring is continued at 80^0C until the complete removal of the solvent. Then degassing and cooling is done in a vacuum oven before mixing with hardener. Subsequently, this solution is mixed with the hardener at a 10:1 ratio, and mechanical stirring of the solution is done for about 2 minutes. To remove the air trapped during the above procedures, degassing in the vacuum oven for approximately 5 minutes is again conducted. Now the degassed solution of GNP epoxy was poured into the silicon moulds under the appropriate DC magnetic field to prepare the test specimens. The same procedure is repeated to synthesize Fe_3O_4-GNP epoxy nanocomposite except that, here, we keep the Fe_3O_4-GNP epoxy solution with THF solvent placed on the hot plate, and simultaneously mechanical stirring is done using a separate attachment. Similarly, the vacuum degassing of the solution is carried out and cured in the silicon mould under a DC magnetic field to cast Fe_3O_4-GNP epoxy nanocomposite test specimens. For the completeness

of the work and comparing the characteristics, neat epoxy specimens were fabricated following the above-stated procedures.

Fig. 4.2 illustrates the nanocomposite fabrication mechanism, which is discussed further in this paper. The cross-linking reaction mechanism of the Epoxy LY-556 and HY- 951 system involves the opening of epoxy groups and amino groups, followed by the linking of chains to form a three-dimensional network structure. This reaction is initiated by the hardener HY-951, which creates covalent bonds with the epoxy groups, resulting in the formation of a highly cross-linked structure. The reaction generates an internal catalyst that aids in adhesion and increases viscosity as the molecules grow longer, forming linear molecular weight. Furthermore, the cross-linking reaction mechanism of the Epoxy LY-556 and HY-951 system, when combined with GNP and Fe_3O_4-GNP, involves the functionalization of the hydroxyl, carboxyl, and epoxide groups of their surfaces with epoxy groups[165]. These groups react with epoxy components, resulting in the formation of a highly cross-linked structure. It is noteworthy that the resulting structure is highly cross-linked, making it more stable and mechanically strong.

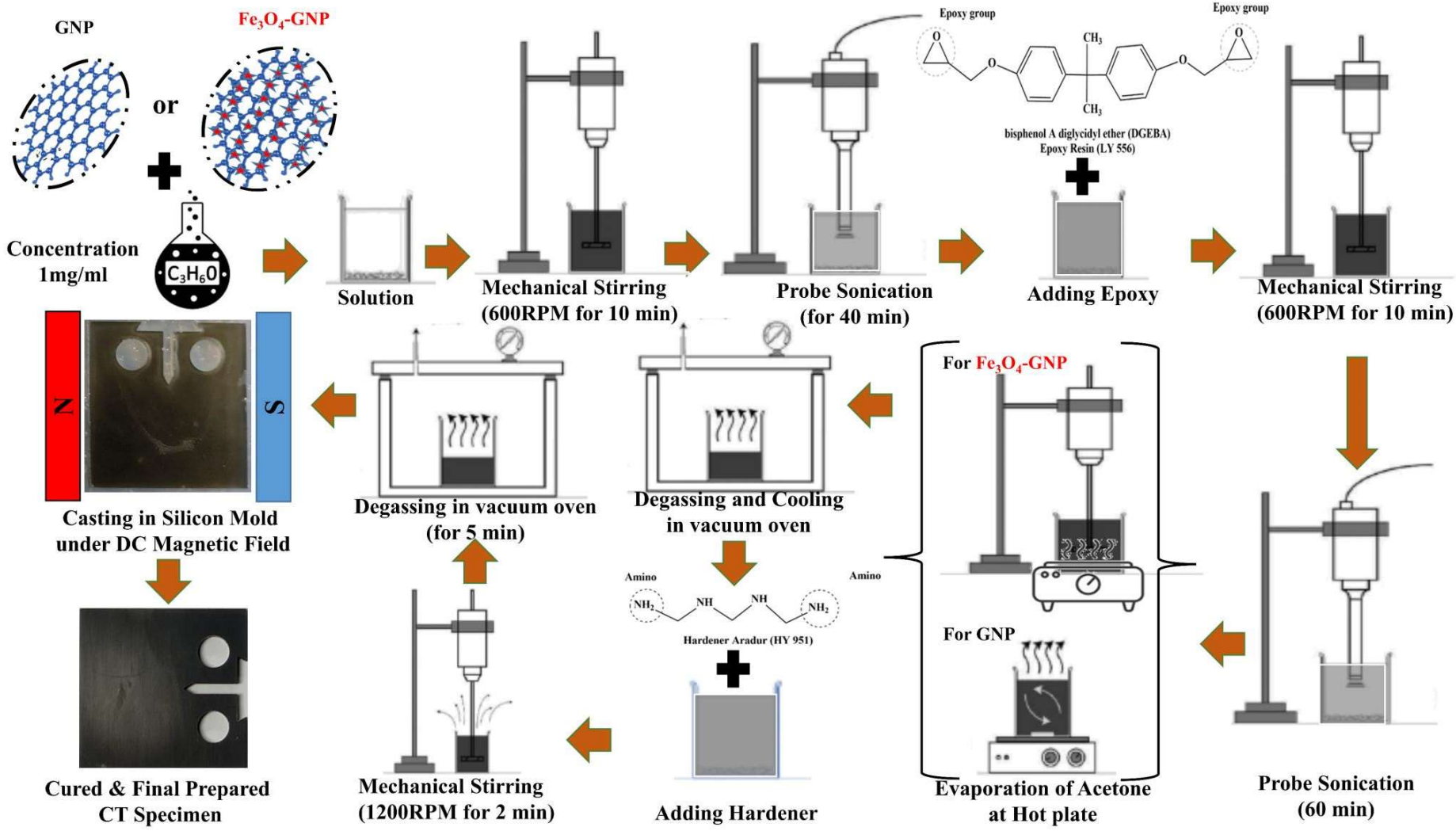

Fig. 4.1. Shows the all steps during fabrication process of the GNP and FE3O4-GNP nanoparticle reinforced nanocomposites.

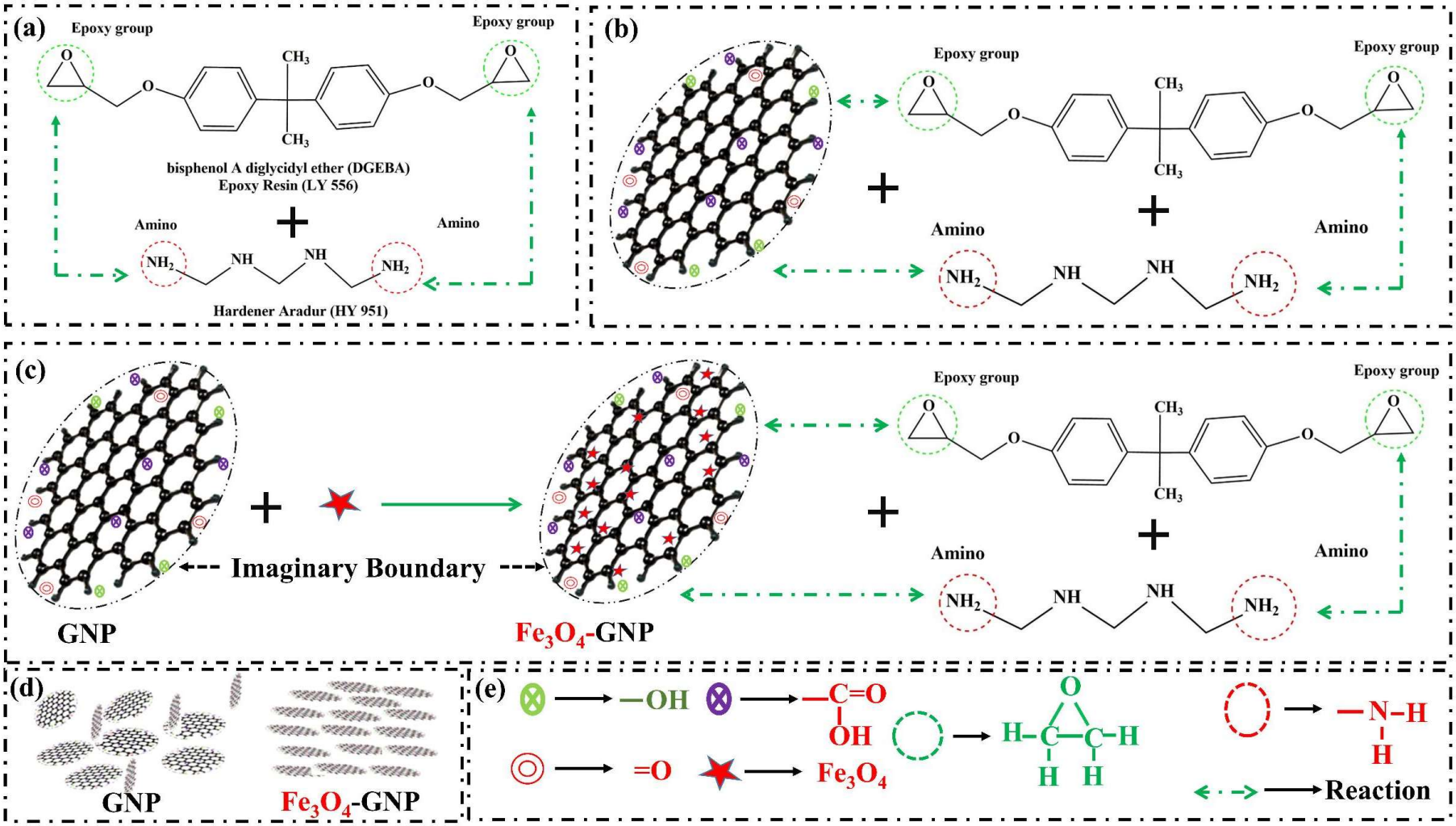

Fig. 4.2. Schematically explain the mechanism of cross-linking reaction of (a) neat epoxy (b) GNP epoxy (c) Fe3O4-GNP epoxy fabrication (d) orientation of GNP and aligned Fe3O4-GNP in epoxy, while, (e) the significance of graphical notations.

4.3. Characterization, morphology and microstructure of GNP, Fe_3O_4-GNP and nanocomposites

4.3.1. HR-XRD (High Resolution X-Ray Diffraction)

The phase analysis, d-spacing, crystal structure, texture, and other structural parameters of GNP, Fe_3O_4-GNP and nanocomposites were characterized by HR-XRD instrument (RigakuSmartLab, RIGAKU Corporation, Japan), using Cu K_α X-ray radiation (wavelength = 1.54059Å) with the tube voltage applied at 40 kV and 15 mA (9kW). The peak profiles were obtained from 10 to 80^o with a 0.020^o step-width. The comprehensive experimental data were analyzed using the X'Pert HighScore Plus software and JCPDS data.

4.3.2. FTIR (Fourier transform infrared spectroscopy)

Figure out the surface functional groups and the bonding among the GNP and Fe_3O_4-GNP. Fourier-transform infrared (FTIR) spectroscopies were performed in 500 cm^{-1} to 4000 cm^{-1} with a resolution of 4 cm^{-1} by FTIR spectrometer (THERMO Electron Scientific, Instruments LLC, Model No: Nicolet iS5).

4.3.3. Raman measurements

nViaRaman spectrometer from Renishaw, UK, was used for Raman spectroscopy to examine the qualitative analysis, formation of chain structure and interaction among the GNP, Fe_3O_4-GNP and epoxy as well as measure the degree of alignment of the Fe_3O_4-GNP nanoparticles in nanocomposite induced by applied magnetic field and polymer stretching.

4.3.4. TGA (Thermogravimetric analysis)

Thermal properties and stability of pure GNP, Fe_3O_4, Fe_3O_4-GNP nanoparticles and their nanocomposites were analyzed by a thermogravimetric analyzer (M/s Shimadzu (Asia Pacific) Pte Ltd, Japan, and Model: TGA-50) using heating rate 10 $^oC\text{-}min^{-1}$ from ambient temperature to 800 ^oC under a nitrogen atmosphere with flow rate of 100 $mL\text{-}min^{-1}$.

4.3.5. DSC (Differential scanning calorimetry)

The curing kinetics and glass transition of epoxy, GNP epoxy, and aligned Fe_3O_4-GNP epoxy have been analyzed via the utilization of a DSC (model DSC-60 Plus, M/s Shimadzu (Asia Pacific) Pte Ltd, Singapore). The sample was carefully placed in an Aluminum pan, and the DSC sample mass was maintained at a precise 5mg. The DSC device was equipped with a liquid nitrogen-based cooling system that operated at a consistent flow rate of approximately 100 mL/min. The samples underwent a dynamic heating scan of 10 °C/min, and were heated within a range of 30-300°C. The resultant DSC curves were analyzed to determine the curing reaction's characteristics.

4.3.6. AFM (Atomic force microscopy)

AFM analysis using Scanning Probe Microscope (SPM) (NTEGRA Prima, NT-MDT Service & Logistics Ltd.) were conducted to determine the three-dimensional structural parameter of GNP and Fe_3O_4, degree of alignments of Fe_3O_4-GNP nanoparticles in epoxy. To create samples for AFM imaging, newly cleaved mica surfaces were coated with a dispersed nanoparticles solution (0.1 mg mL^{-1}) and left to dry in the air. The post-fracture surface roughness of GNP, Fe_3O_4-GNP nanoparticles nanocomposites were also evaluated at random location.

4.3.7. XPS (X-ray photoelectron spectroscopy analysis)

The chemical state and quantitative information of GNP and Fe_3O_4-GNP's surfaces and interaction between Fe_3O_4 and GNP were determined by X-ray photoelectron spectroscopy

analysis using Al Kα source (engery 1486 ev) and providing a pass energy of 200ev) (K-Alpha, Thermo Fisher Scientific).

4.3.8. BET (Brunauer–Emmett–Teller) analysis

BET analysis with ELLSORP MAX II & BELCAT-II (Microtrac BEL Corp.) was carried out to determine the specific surface area and the pore size distribution of GNP and Fe_3O_4-GNP by measuring N2 adsorption-desorption at 77 K.

4.3.9. Exploration of the alignment of the Fe_3O_4-GNP

A weak magnetic field was applied to a liquid mixture of Fe_3O_4-GNP and epoxy that included 0.05 wt % of Fe_3O_4-GNP, and the movement of the mixture's Fe_3O_4-GNP was monitored using a dewinter optical microscope for the required period of time.

4.3.10. HR-SEM and HR-TEM analysis

In order to investigate the morphologies of GNP, Fe_3O_4-GNP, element composition and dispersion of nanoparticles in its nanocomposites as well as the fracture surfaces, the nanocomposites were characterized using a High-Resolution Scanning Electron Microscope (HR-SEM) (FEI Company of USA (S.E.A.) PTE, LTD, Model: Nova Nano SEM 450) equipped with EDXMA (Energy dispersive X-ray microanalysis) (Team Pegasus Integrated EDS-EBSD with Octane Plus and Hikari Pro,). The morphologies, particles size and dispersion of Fe_3O_4 on GNP surfaces, were analyzed using a HR-TEM (High Resolution Transmission Electron Microscope) analysis, using Tecnai G2 20 TWIN (FEI (S.E.A.) PTE, LTD).

4.3.11. Chemorheological behaviours of epoxy during curing

A rheometer MCR302 (Anton Paar, Austria) with parallel plate attachment was used to determine the dynamic chemorheological characteristics of epoxy during the curing process. The Viscosity test was conducted at room temperature (30°C) in dynamic strain sweep (rotary) mode, with a shear rate of 50 s^{-1}.

4.3.12. Measurement of magnetic properties

To study the magnetic characteristics, magnetic hysteresis loops were recorded at room temperature (300 K) using a Vibrating Sample Magnetometer (Quantum Design, USA).

4.4. Results and discussion

The mathematical model for the time required for the alignment process was developed, and the experimental approach validated it. The physical, chemical and Fe_3O_4 nanoparticle attachments to the GNP surface are all examined using the characterization methods listed below. The mathematical model's optimized parameters are also used to complete the entire alignments, and the alignments are then confirmed using the following methods.

4.4.1. HR-XRD analysis

The crystal structure and phase composition of the GNP, Fe_3O_4, Fe_3O_4-GNP and the nanocomposites were characterized by HR- XRD. As shown in **Fig. 4.3 (a)**, The XRD pattern for GNP indicates a strong diffraction peak at 2θ ~26.70°[166,167] which can be attributed to the (002) crystal plane of the graphitic structure, corresponding to an intergraphenes d-spacing of about 0.3354 nm as per JCPDS 75–1621. For Fe_3O_4, the peaks at 2θ ~30.30° , 35.60° , 43.30° , 30.30° , 53.60° , 57.10° and 62.90° can be discerned, which are allocated to the diffraction of (220), (311), (400), (422), (511) and (440) planes of the magnetic Fe_3O_4, respectively.

Furthermore, in the XRD pattern of Fe_3O_4-GNP, the peak corresponding to 2θ ~26.70° matched to the GNP(i.e., carbon nanomaterials[168]) and others compared with characteristics peaks of the Fe_3O_4. This advised that the Fe_3O_4 nanoparticles are anchored on the GNP, and the heterostructure is formed. XRD data also supported the alignment of Fe_3O_4-GNP within the epoxy. A very intense peak is visible at $2\theta = 19.46^0$ in **Fig. 4.3 (b)** diffraction from the top plane of the highly organized Fe_3O_4-GNP nanocomposite. The scattering from Fe_3O_4-GNP planes parallel to the direction of the magnetic field causes a strong peak. On the other hand, the diffraction patterns exhibit substantially weaker peaks in nanocomposites when GNP is randomly oriented in epoxy. The concentration of Fe_3O_4-GNP planes that meet Bragg's equation at $2\theta = 19.46^0$ is directly correlated with the diffraction peak strength, as is evident, which demonstrates that the alignment was successful.

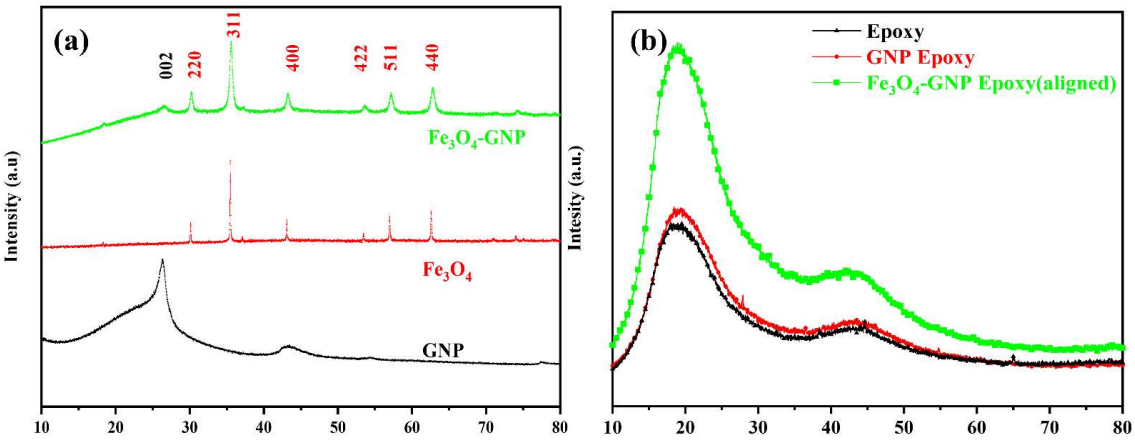

Fig. 4.3. Shows the comparative X-ray diffraction of (a) GNP, Fe_3O_4, and Fe_3O_4-GNP and (b) epoxy, GNP epoxy and Fe_3O_4-GNP epoxy nanocomposites.

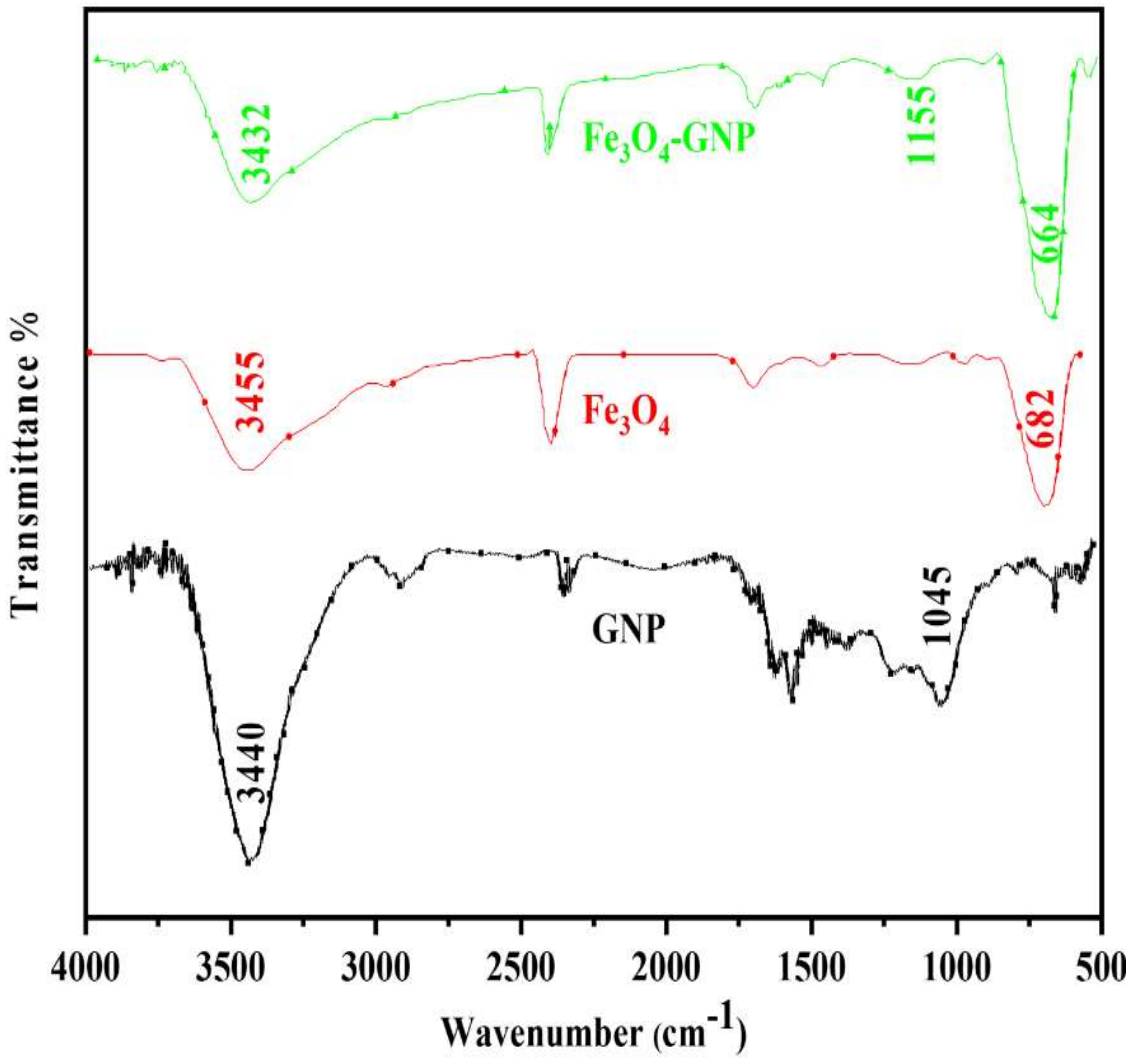

Fig. 4.4. Shows the comparative Fourier-transform infrared spectroscopic (FTIR) analysis of GNP, Fe_3O_4, and Fe_3O_4-GNP.

4.4.2. FTIR (Fourier transform infrared spectroscopy)

The **Fig. 4.4**, shows the comparative Fourier-transform infrared spectroscopic (FTIR) analysis of GNP, Fe_3O_4, and Fe_3O_4-GNP to confirm the functional groups on their surfaces and validate the formation of bonding between GNP and Fe_3O_4. In the IR spectrum of GNP, the observed typical peaks in GNP approve the existence of oxygen-containing functional groups in carbon frameworks. The stretching vibration of the peaks are occurred at 1045 cm^{-1} for epoxide (C-O-C group), 1392 cm^{-1} for carboxylic acid (C-OH groups), 1620 cm^{-1} (C=C in the aromatic ring) and 1706 cm^{-1} for carbonyl and carboxyl groups (C=O) at the edges of GNP. As well as, due to the presence of the carboxylic acid group (O–H), a tough and wide stretching vibration at 3440 cm^{-1} can be seen[169–171]. From the Fe_3O_4 spectra, a sharp peak is observed at about 682 cm^{-1} (the bending bond) characteristics of the Fe–O bond absorption, and also, a peak at 3455 cm^{-1} seen corresponding to the hydrogen bonds in water, which endorses the presence of the magnetic core[172]. The IR spectra of Fe_3O_4-GNP show the characteristics and differences between GNP and Fe_3O_4.

4.4.3. Raman spectroscopy

The crystalline, nanocrystalline, and amorphous graphitic base materials are usually investigated by the Raman spectrum[173,174]. In **Fig. 4.5 (a),** the Raman spectrum of GNP, Fe_3O_4, and Fe_3O_4-GNP are described from wave number 500 cm^{-1} to 1800 cm^{-1}. For the Fe_3O_4 Raman spectrum, the small band is seen at 686 cm^{-1} and this characterizes modes conforming to Fe-O stretching. This weak Raman scattering of the Fe_3O_4 confirms its magnetite state[175]. There are two prominent peaks in the Raman spectrum for GNP and Fe_3O_4-GNP, except for Fe_3O_4. These two important intense features are known as D-band and G-band,where the D-band relates to the degree of disorder (or defects) of the sp^3-hybridized carbon structure of the E_2g mode, and while the G band is indorsed to in-plane vibrations of the sp^2-hybridized carbon atoms with in-plane A_1g zone-edge mode (graphite structure)[173]. The D-band of the GNP

and Fe_3O_4-GNP are seen at 1312, and 1532 cm^{-1}, while the G-band is located at 1323 and 1550 $cm^{-1,}$ respectively.

However, the intensity of the D-band of both materials is weak compared to their respective G band, which specifies a small fraction of defects' presence. Hence, the level of defects in the graphene-related materials can be characterized by the I_D/I_G ratio in Raman spectra[176]. The implanted Fe_3O_4 on the GNP would undeniably impact the wave function of the optical photons not only from the relaxation of the selection rule

but also from the surface strains ascribed to the Fe_3O_4 functional on GNP. Consequently, the two peaks of the Fe_3O_4-GNP are broadened and shifted toward the higher wave number compared to GNP[175]. Raman spectroscopy is used to evaluate the degree of Fe_3O_4-GNP alignment further. This approach is predicated on the concept that carbon materials' tangential mode Raman intensities are strongly polarisation angle-dependent. As a result, if the Fe_3O_4-GNP are aligned, the strength of the Raman peak is dramatically increased parallel to the polarised laser excitation plane[173,177]. **Fig. 4.5 (b)** shows the Raman spectroscopic analysis of neat epoxy, GNP nanocomposite and aligned Fe_3O_4-GNP nanocomposite under the weak magnetic field. Additionally, it is observed that the Raman band intensities of the neat epoxy and the two types of nanocomposites differ noticeably, with the Fe_3O_4-GNP nanocomposite exhibiting a significantly higher intensity than the GNP nanocomposite and neat epoxy perpendicular to the direction of magnetic alignment. This further illustrates that our magnetic alignment strategy can successfully produce a good alignment of the Fe_3O_4-GNP in the nanocomposite.

4.4.4. TGA (Thermogravimetric analysis)

The TGA thermograms of the nanoparticles are displayed in **Fig. 4.6 (a)**. For the GNP, Fe_3O_4, and Fe_3O_4-GNP, the slight weight loss (~3.45, 3.31 and 2.67, respectively) took place between the ambient temperature and ~150°C. The weight loss below ~150°C can be attributed to the

desorption of physically-absorbed H_2O, solvent, pyrolysis of the oxygen-containing group and the slow decomposition of the thermally unstable nanoparticles. The deterioration of GNP speeded up around 150-250°C due to an exothermic reaction and weight loss between this temperature range ~7.81%. This symptom links to the decomposition of oxygen-containing functional groups to CO_2. The 6.69 % weight loss of Fe_3O_4-GNP for the temperature range ~150°C -360°C) corresponds to the oxidation and breakdown of the bond between GNP and Fe_3O_4. The pyrolysis of the carbon skeleton of the GNP has occurred between ~250°C and 500°C. The 5.24% weight loss as result of releasing the CO, CO2 and H2O and finally, the hefty weight loss (~12.21%) at ~500°C-700°C is attributed to the oxidation and full combustion of the carbon skeleton of the GNP[178,179]. The mild weight gain (~0.35%) in the thermograms of Fe_3O_4 is observed due to the oxidation of magnetite (Fe_3O_4)[180]. Even over 800 °C, the weight loss of Fe_3O_4 and Fe_3O_4-GNP is 6.17% and 11.09%, respectively. Therefore, the mass loading of Fe_3O_4 in the Fe_3O_4-GNP can be calculated as 88.91%.

The study illustrates **Fig. 4.6 (b)** with the thermal decomposition curves of cured epoxy, GNP epoxy, and Fe_3O_4-GNP epoxy. Notably, a single sharp weight-loss stage occurs at around 300-450^0C in all samples, attributed to the chain break-down of the polymer structure. The incorporation of nanofillers in the epoxy resin leads to a decrease in decomposition temperature, likely due to the nanoparticles' obstruction on the formation of the high cross-linked molecular structure of epoxy[181]. However, it is observed that GNP epoxy has a higher onset decomposition temperature than Fe_3O_4-GNP epoxy, indicating that the Fe_3O_4 nanoparticles on the surface of GNP have an adverse impact on the epoxy's thermal stability. Additionally, the Fe_3O_4-GNP epoxy has lower weight loss than the epoxy and GNP epoxy during the 450-800^0C heating range. The protruding Fe_3O_4 nanoparticles on the surface of GNP in the Fe_3O_4-GNP epoxy promote char formation during thermal degradation, which is likely responsible for the reduced weight loss[182].

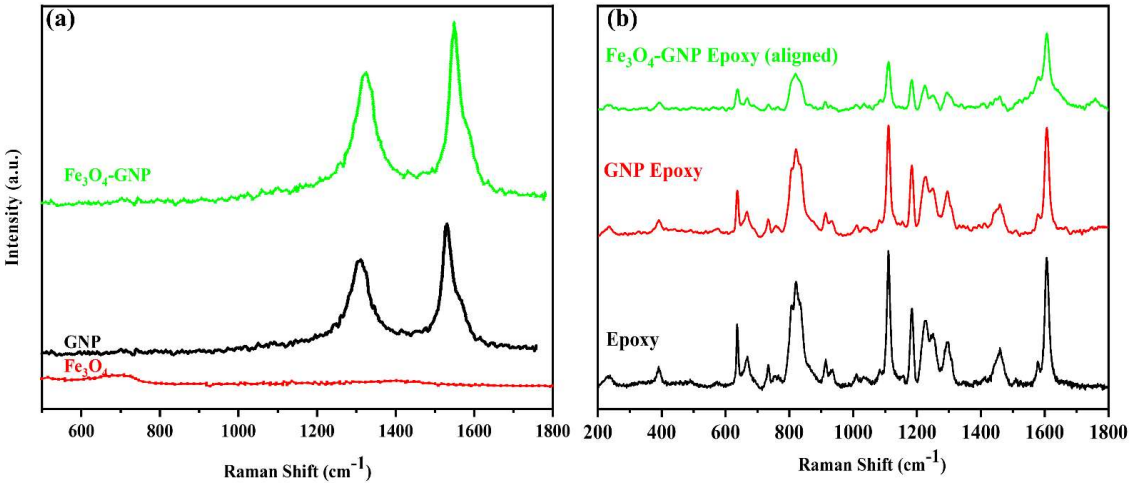

Fig. 4.5. Shows the comparative Raman spectroscopic analysis of (a) GNP, Fe_3O_4, and Fe_3O_4-GNP; and (b) epoxy, GNP epoxy and Fe_3O_4-GNP epoxy.

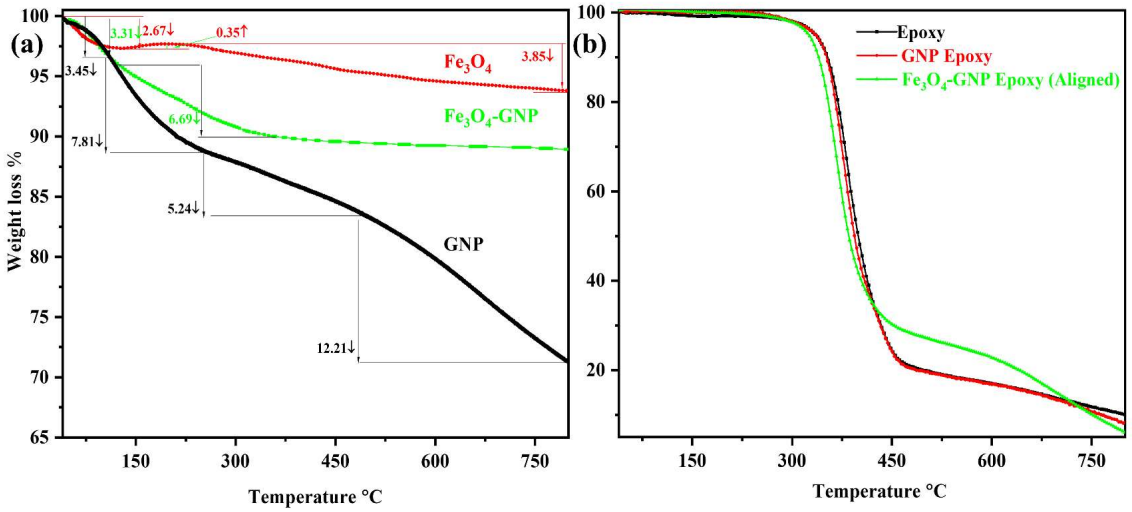

Fig. 4.6. Describes the comparative thermogravimetric analysis (TGA) of (a) GNP, Fe_3O_4, Fe_3O_4-GNP and (b) their nanocomposites.

4.4.5. DSC (Differential scanning calorimetry)

The DSC thermograms **(Fig 4.7**) have revealed important insights into the curing behaviour and glass transition temperature of epoxy, GNP epoxy, and aligned Fe_3O_4-GNP epoxy. Notably, the measurements have demonstrated that the GNP epoxy and Fe_3O_4-GNP epoxy exhibit a

lower Tg than the epoxy, attributable to the enlarged free volume resulting from the interface between the fillers and the epoxy resin[183](**Fig 4.7 (a)**). This has facilitated greater movement of the polymer chain segments, even at lower temperatures, as well as the formation of interrupted cross-linking networks in the nanocomposites, resulting in a reduced Tg. The reduction in Tg owing to the addition of fillers is believed to result mainly from the nanoparticle's catalytic effect on the curing reaction, with the hydroxyl, carboxyl, and epoxide groups on GNP and Fe_3O_4-GNP serving as catalysts to speed up the curing reaction by participating in the opening of the epoxide ring, similar to an amino curing agent[184]. One possible explanation for the decrease in Tg could be the increase in viscosity resulting from the presence of GNP and Fe_3O_4-GNP sheets, which could lower the mobility of the reactive species. Another contributing factor could be that the sheets of nanoparticles have impeded the degree of cure reaction to some extent.

However, When the temperature is increased beyond the glass transition temperature (Tg) during the DSC test, the polymer segments can move, and the curing process is accomplished, leading to an additional curing process observed in the DSC curve (**Fig 4.7 (b)**). The residual heat of the curing can be used to calculate the curing extent. The Fe_3O_4-GNP nanoparticles,

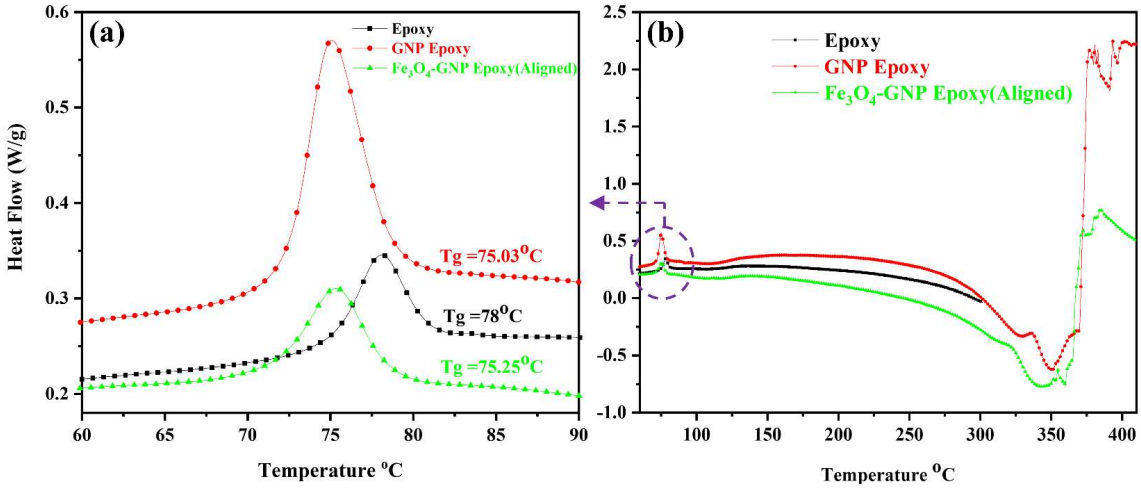

Fig 4.7. Explains the DSC thermograms of epoxy, GNP epoxy and aligned Fe3O4-GNP epoxy at constant heating rate 10°C/min. (a)The glass transition temperature (Tg) is mentioned with each thermograms and (b) Higher heating

which have rougher surfaces due to the presence of Fe_3O_4 nanoparticles on the GNP surface, provide more free volume than GNP, resulting in a higher curing extent. Therefore, the DSC test is a fast, sensitive, and easy-to-use method for identifying kinetics and characterizing materials by measuring enthalpy changes due to changes in the physical and chemical properties of a material as a function of temperature or time[185].

4.4.6. XPS (X-ray photoelectron spectroscopy analysis)

The presence of Fe, C and O in the synthesized sample is confirmed from XPS survey spectrum shown in **Fig. 4.8**. Further, the oxidation states of the Fe in the sample are analyzed through high-resolution XPS spectra, which indicates its multivalent ionic state. **Fig. 4.8 (e)** displays the HR-XPS spectra of C1s in the procured graphene sheets. The peak ~284.6 eV corresponds to sp2 hybridized C in the graphene. The HR-XPS spectra of C1s in the synthesized material also display a similar feature which confirms that the graphene's phase integrity is maintained and did not oxidize during the synthesis. The HR-XPS spectrum of O1s in graphene is shown in **Fig. 4.8 (c)**. The deconvoluted O1s peaks with binding energies of 531.2, 532.1 and 533.3 eV represent the O-C=OH, C=O and C-OH, respectively, of the graphene phase. These three peaks also exist in the O1s XPS spectrum of the prepared sample in addition to a peak at 530.3 eV due to the Fe-O bond. The HR-XPS scan of Fe 2p in the sample closely resembles that of Fe_3O_4 [186]. Due to spin-orbit coupling, the XPS spectrum of Fe has split into two envelops, i.e., Fe 2p3/2 and Fe1/2. The corresponding Fe 2p3/2 and Fe1/2 envelopes are positioned around ~711.0 eV and 724.6 eV, respectively. A flat satellite feature was observed which is due to the cumulative contribution from Fe^{2+} at 715.4 eV and Fe^{3+} at 719.3 eV. The Fe 2p3/2 spectrum is de-convoluted with three sub-peaks. The peaks at 709.9 eV is due to Fe^{2+} at octahedral position while the peaks at 711.2 and 713.1 eV are due to Fe^{3+} coordinated to octahedral and tetrahedral environments, respectively.

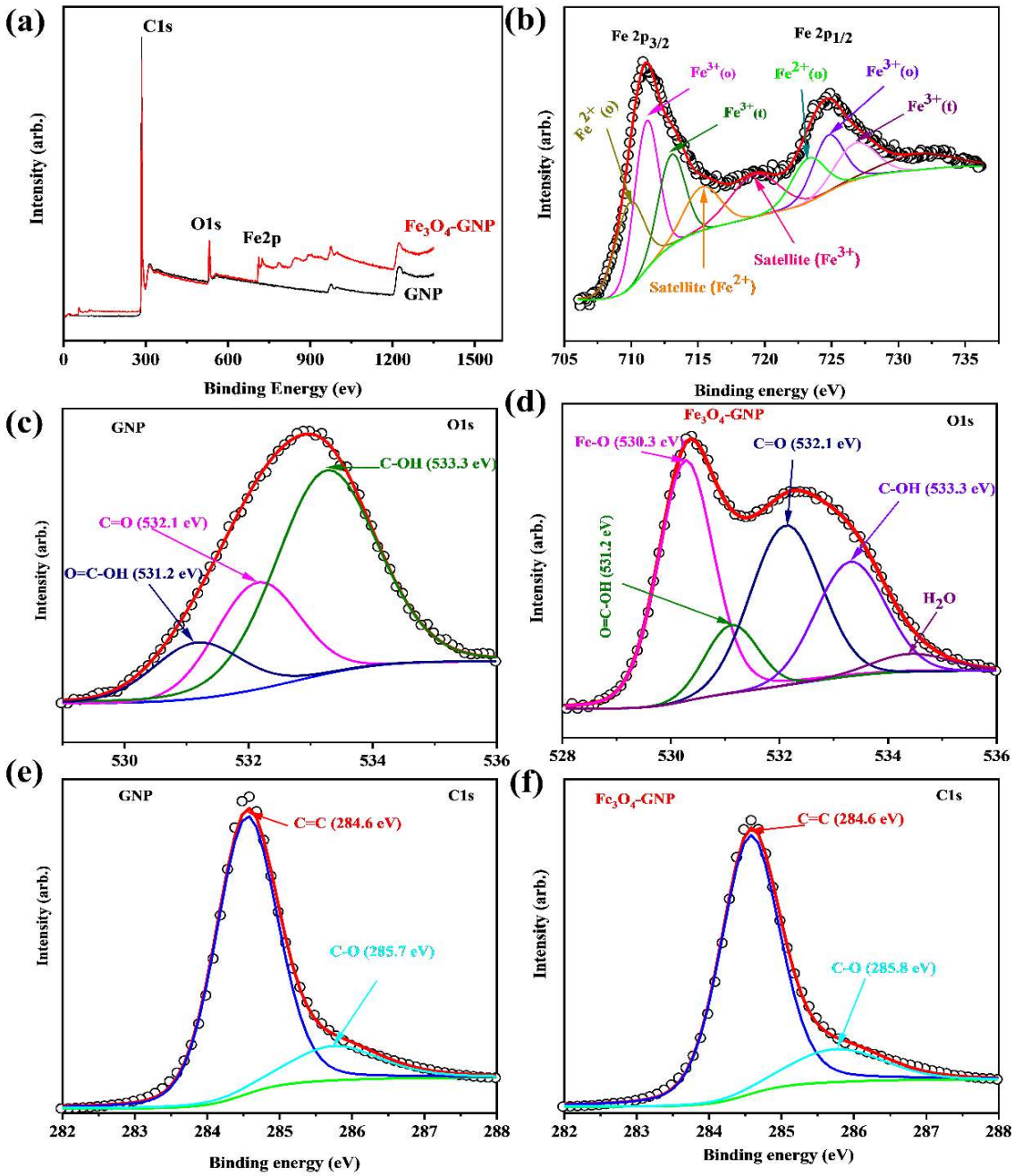

Fig. 4.8 show (a) survey spectrum of the GNP and Fe_3O_4-GNP;(b) high resolution Fe2p scan of the Fe_3O_4-GNP; (c) and (d) High-resolution O1s scans of GNP and Fe_3O_4-GNP, respectively; and (d) and (f) high resolution C1s scans of GNPs and Fe_3O_4-GNP.

4.4.7. BET (Brunauer–Emmett–Teller) analysis

To measure the surface area and recognize the physical structure of solid or porous materials BET is applied. **Fig. 4.9 (a)** shows N2 adsorption and desorption isotherms characteristic of mesoporous-like material that have multilayer pores, which is confirmed by the plateau and an H3 hysteresis loop[187]. The BET yields specific surface areas of 705 m^2/gm for GNP and 467 m^2/gm for Fe_3O_4-GNP, respectively. This decrease in the BET surface area of Fe_3O_4-GNP provides indirect evidence for grafting Fe_3O_4. It can be shown that when GNP is modified, there is a decline in adsorbed volume for Fe_3O_4-GNP at low relative pressure. BET surface area, and pore size distribution (**Fig. 4.9 (b)**) and cumulated surface area (**Fig. 4.9 (c)**), can all be used to quantify the effect of organic molecules grafting on graphene sheets.

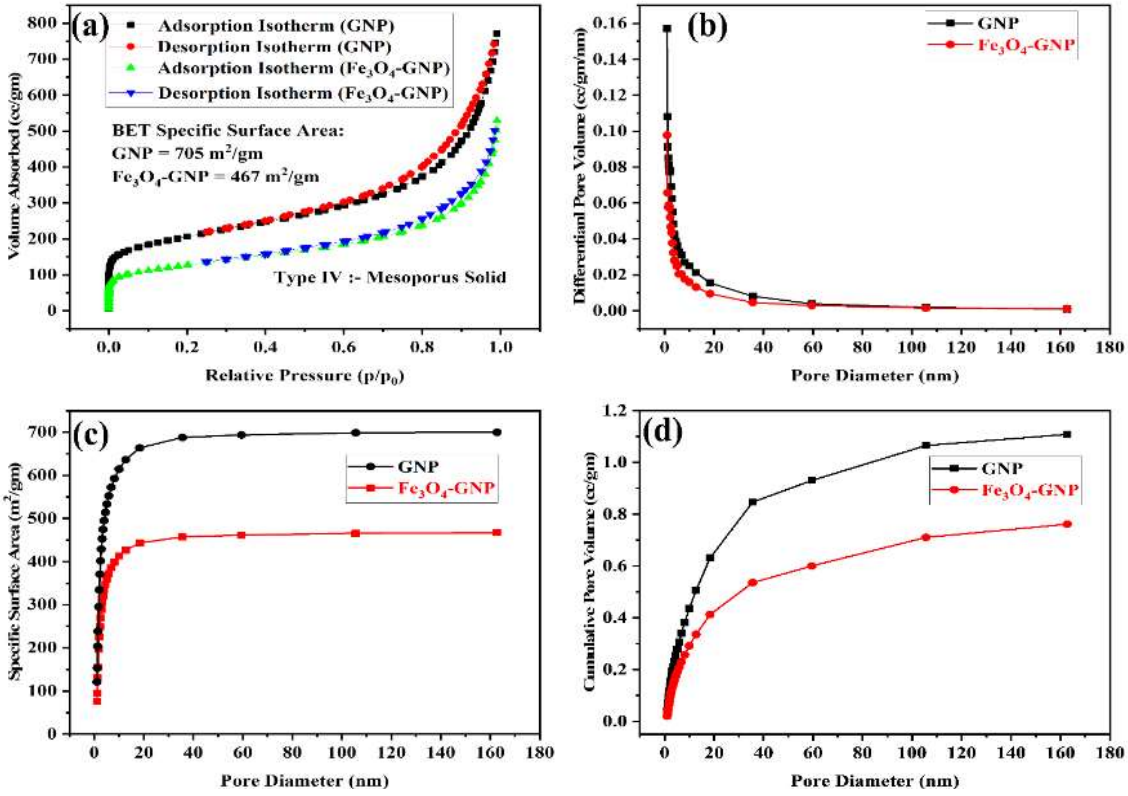

Fig. 4.9. Shows (a) N2 adsorption and desorption isotherms (b) BJH isotherm curves (by adsorption) (c) cumulated surface area vs. pore diameter and (d) cumulated pore volume vs. pore diameter of GNP and Fe_3O_4-GNP.

4.4.8. Exploration of the alignment of the Fe_3O_4-GNP

Fig. 3.9 depicts optical microscope pictures of the Fe_3O_4-GNP/epoxy microstructure (0.05 wt %) in a weak magnetic field. The images are taken before curing as well as after the curing process. As anticipated, Fe_3O_4-GNP in the epoxy changes orientation over time and aligns with the direction of the applied magnetic field. Most of the Fe_3O_4-GNP in the most recent images are positioned nearly parallel to the applied magnetic field. We demonstrated that aligning the Fe_3O_4-GNP in an epoxy resin using a very low magnetic field can be a successful substitute for doing so with a large magnetic field. For much practical mechatronics and electrical devices, a high magnetic field seems impractical and limits the utility of the equipment for the GNP base functional materials.

4.4.9. SEM and TEM analysis

Scanning electron microscopy and transmission electron analysis were used to explore further the microstructure and morphology of the GNP and Fe_3O_4-GNP nanoparticles and hybrids, and the results are given in **Fig. 4.10** and **Fig. 4.11**, respectively. GNP are platelet-shaped agglomerated particles of multiple graphene layers layered on each other[188]. Small Fe_3O_4 nanoparticles were found to be grafted on GNP, resulting in a markedly altered morphological structure of Fe_3O_4-GNP. The **Fig. 4.11 (e)** show that the produced Fe_3O_4 nanoparticles have a spherical shape with particle sizes ranging from 165 to 265 nm. The GNP particles have a platelet-like shape with smooth surfaces, as observed. The Fe_3O_4-GNP, on the other hand, has platelets that appear to be covered in Fe_3O_4 nanoparticles. TEM examination confirmed the attachments of Fe_3O_4 nanoparticles. It was clear that the Fe_3O_4 nanoparticles had been efficiently bound to the GNP, particularly at the GNP edges. The existence of C, Fe, and O elements in the hybrid samples was confirmed by energy dispersion spectroscopy analysis (EDS), indicating that the Fe_3O_4 nanoparticles were fixed onto the GNP surface in the hybrids.

The fracture surfaces of the nanocomposites were also examined using SEM, and typical images of SEM and its 3D patterns are shown in **Fig. 4.12** . The nanocomposite's fracture surface has a higher roughness than neat epoxy, indicating strong filler-matrix interfacial interactions[189]. The fracture surface of the neat epoxy illustrates usual brittle fracture characteristics and wrinkle-like texture or "river-like" fracture patterns initiated by the cracks (**Fig. 4.12 a** and **c**). The crack propagated quickly in the neat epoxy after it was initiated, just like any other usual brittle material. This river bed-like pattern developed from various micro-cracks that are combined/expanded, while the area between these patterns is extremely smooth, indicating a

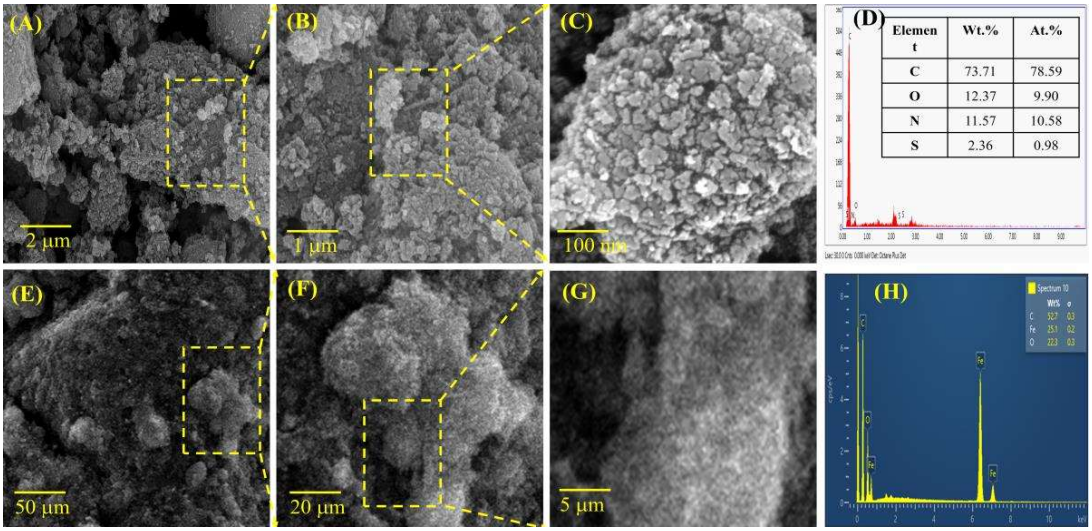

Fig. 4.10. Show (a) the surface morphology of the GNP, (b) a particle of the GNP, (c) the particles size distribution and (d) elemental analysis of the GNP

high propagation velocity[53,190,191]. The ductile ripping of the polymer by void nucleation and growth is the result of neat epoxy's crazing fracture mechanism. The voids in pristine epoxy originate in the polymer's intracrystalline regions. The weakest points of the material are these intracrystalline areas[192]. Similar "river-like" fracture patterns may be seen on the fracture surface of the GNP epoxy nanocomposite, in contrast, a very different fracture morphology is observed in the **Fig. 4.12** (**c** and **d**). The fracture surface appears to be smoother in a low-magnification image than in a high-magnification image and 3D image **Fig. 4.12** (**c and d**). Still, the high-magnification image and the 3D patterns demonstrate that considerable surface

roughness was formed. As a result of the GNP acting as blockades against the rapid crack propagation, the surface appears more ductile. Because the GNP/epoxy interphase is the weakest ligament in the material and is where microcracking tends to propagate, crack branching and subsequent ditching show that there is a higher crack resistance to microcracking. In order to pass the GNP and Fe_3O_4-GNP, the cracks must tilt or twist at greater angles. As a result, more peaks and valleys would form on the fracture surface of GNP and Fe_3O_4-GNP epoxy nanocomposites [**Fig. 4.12 (d)** and **(f)**] The SEM and 3D image pattern of the nanocomposites' fracture surfaces show good dispersion and homogeneity of GNP and Fe_3O_4-GNP, with almost no restacks of these nanoparticles in either nanocomposite. Furthermore, the fracture surface and 3D image pattern of the Fe_3O_4-GNP nanocomposites clearly show a significant alignment of Fe_3O_4-GNP in the direction of magnetic field.

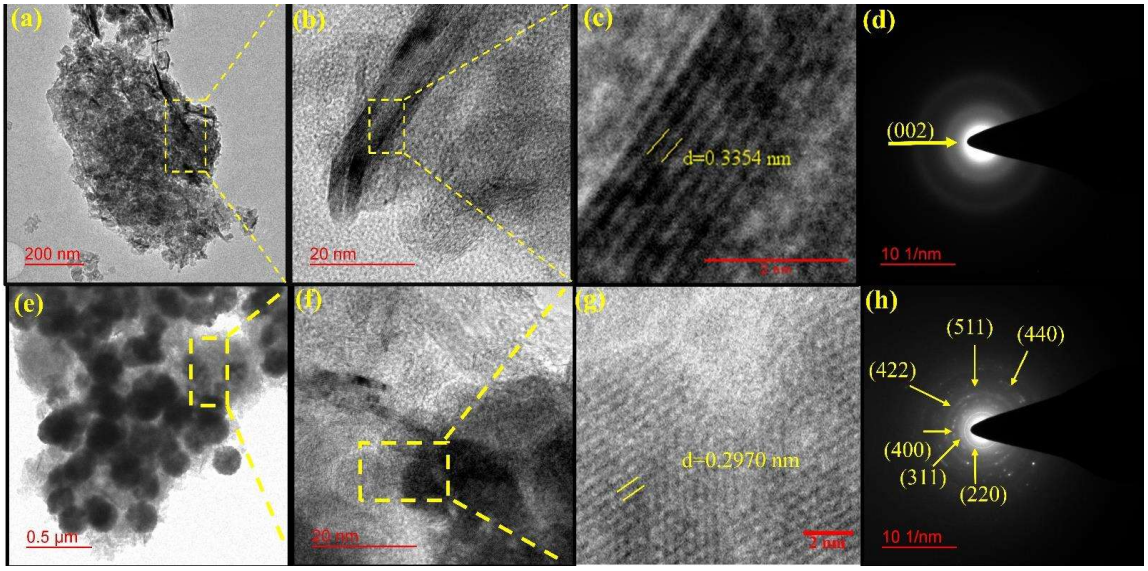

Fig. 4.11. Illustrate TEM of GNP and Fe_3O_4-GNP nanoparticles. (e) Fe_3O_4-GNP nanoparticles show that Fe_3O_4 particles are attached on the GNP surfaces; (c) SAED pattern showing the nanoparticles structure, where the lattice planes of GNP and Fe_3O_4-GNP are clearly visible.

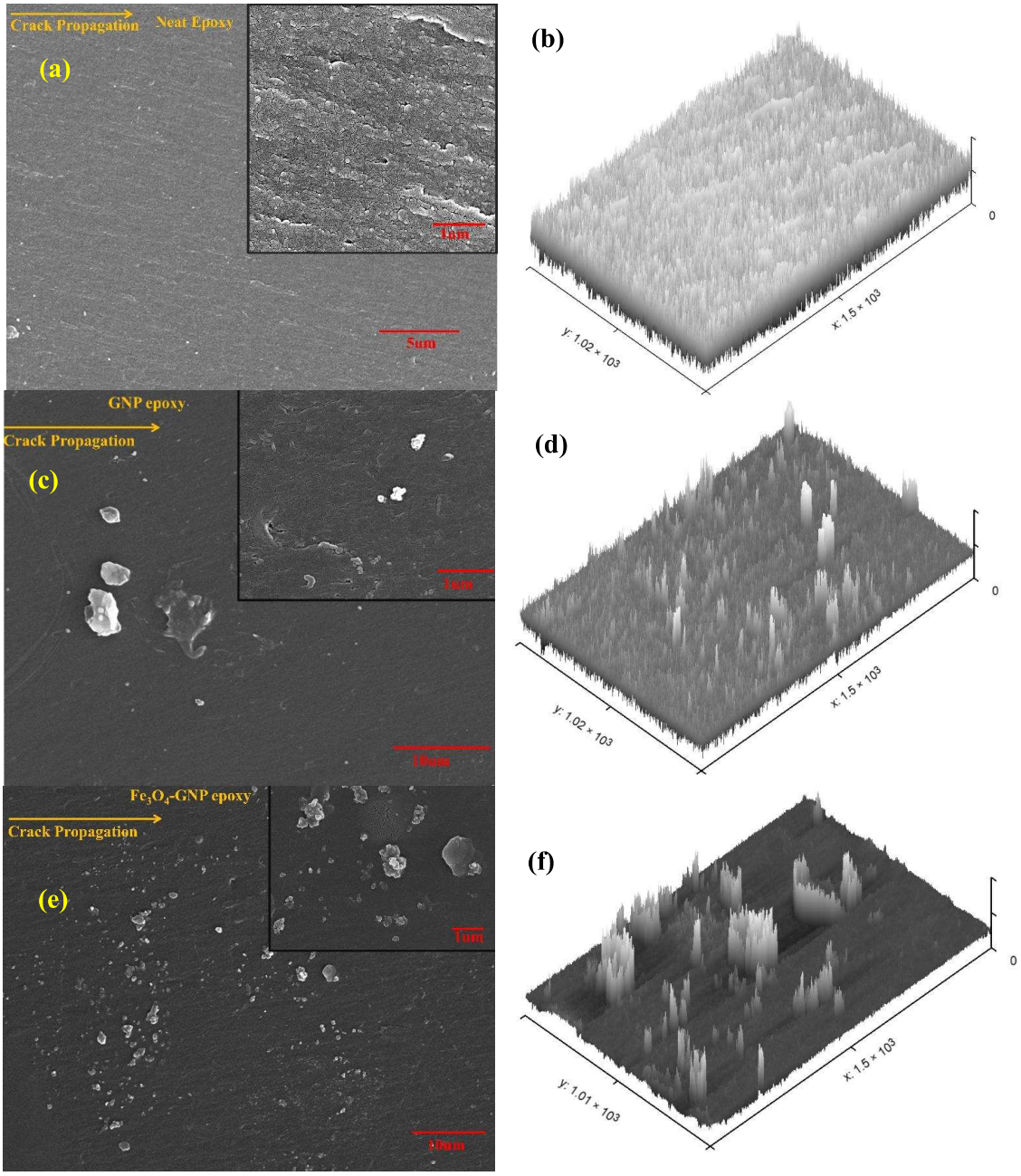

Fig. 4.12. Shows the (a), (c) and (d) SEM images of fracture surfaces and (b), (d), (f) the relative fracture surfaces nature.

4.4.10. AFM analysis

Fig. 4.13 (a) and **(e)** show an illustration of nanoparticles deposition on a mica substrate captured using the standard AFM tapping mode, which reveals that the particle size of GNP are bigger than Fe_3O_4-GNP. The size reduction in the Fe_3O_4-GNP is due to the sonication of GNP during the synthesis process. **Fig. 4.13 (b)** and **(f)** in this part of the figure, the particle size distribution of the nanoparticles is shown in the histogram with a gaussian distribution. By observing the distribution, we concluded that the size of GNP and Fe_3O_4-GNP are 0.5 μm and 0.28 μm, respectively which was also confirmed by Dynamic light scattering particle measurement shown in **Fig. 4.15**. The part of **Fig. 4.13 (c)** and **(g)** shows the 3D roughness of single surface of the nanoparticles. We can easily confirm that the shape of the GNP nanoparticles are like oblates and after Fe_3O_4 attachments to nanoparticles oblate nature of shape has improved. This has also been in accordance with the mathematical model, where the shape is considered as an oblate. The last part of **Fig. 4.13 (d)** and **(h)** demonstrates the surface texture of the GNP and Fe_3O_4-GNP, respectively. The surface texture expresses the roughness, texture and waviness of Fe_3O_4-GNP are more than GNP because of Fe_3O_4 attachments[193]. We concluded that crumbled nature, waviness and oblate nature of GNP enhanced after the attachments of Fe_3O_4 nanoparticles.

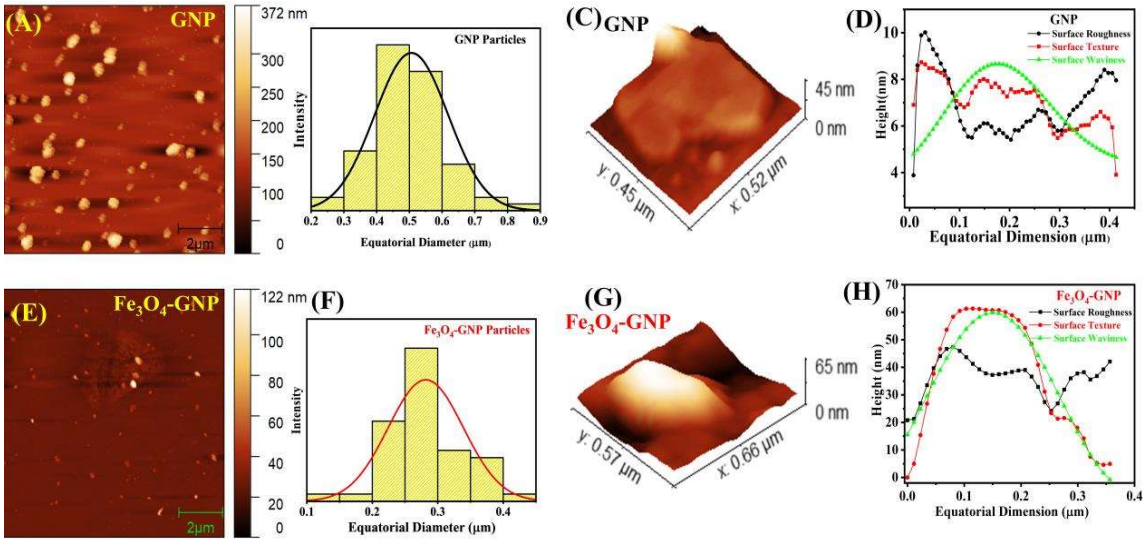

Fig. 4.13. Shows (a) and (e) an illustration of nanoparticles deposition on a mica substrate captured using the standard AFM tapping mode, (b) and (f) particles size distribution, (c) and (g) 3D roughness of single surface, (d) and (h) surfaces texture of the GNP and Fe_3O_4-GNP, respectively.

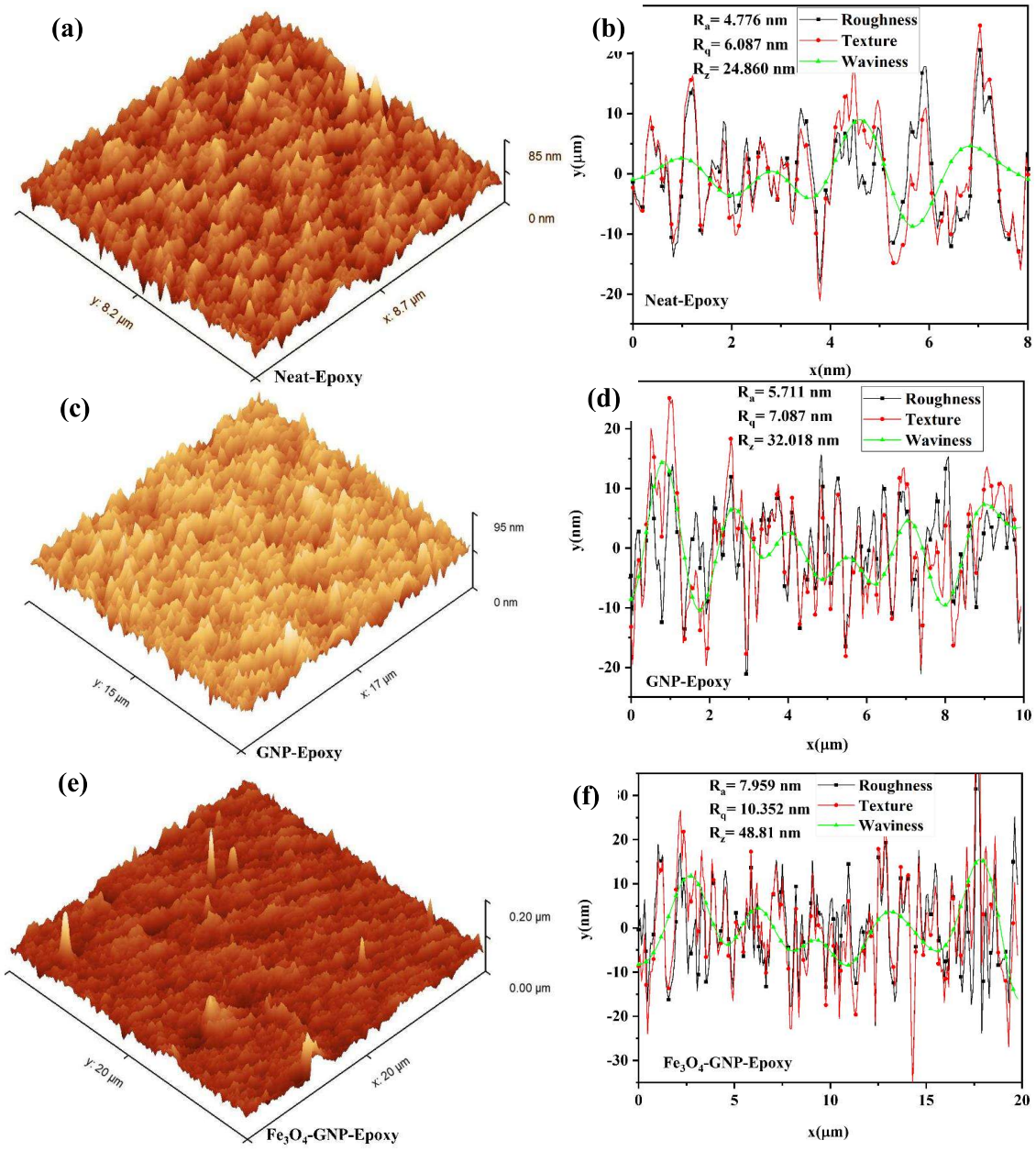

Fig. 4.14. Shows (a, c, e) the 3D roughness profile and (b, d, f) surface roughness parameters of the fracture surfaces of the nanocomposite.

To measure alignment, particle arrangements, and fracture energy through crack deflection observation, **Fig. 4.14.** provides the average values of typical fracture surface roughness morphology for neat epoxy, GNP-epoxy, and Fe_3O_4-GNP -epoxy nanocomposites. The surface roughness is denoted by basically three parameters R_a, R_q and R_z, over a line, which is defined further. The roughness parameter R_a is the most commonly used amplitude parameter for calculating the arithmetic average of vertical deviations from a reference surface line. R_q is the

profile heights' root mean squared evaluation length average. At the same time, R_Z is the mean value of the absolute heights of the five most prominent peaks and the five deepest valleys within the evaluation length. For various nanocomposites, as can be observed, the surface's roughness increases. The nanocomposite materials neat epoxy, GNP epoxy, and Fe_3O_4-GNP epoxy have rougher surfaces in a progressive sequence. The obtained average roughness parameters are shown in **Table 4.1**. Compared to GNP epoxy nanocomposites, aligned Fe_3O_4-GNP nanocomposites appear to have a higher particle-crack interaction for the same volume fractions. When nanoparticle nanocomposites are aligned, this makes the crack travel along a more convoluted course, creating more surface area and increasing the amount of energy lost during fracture.

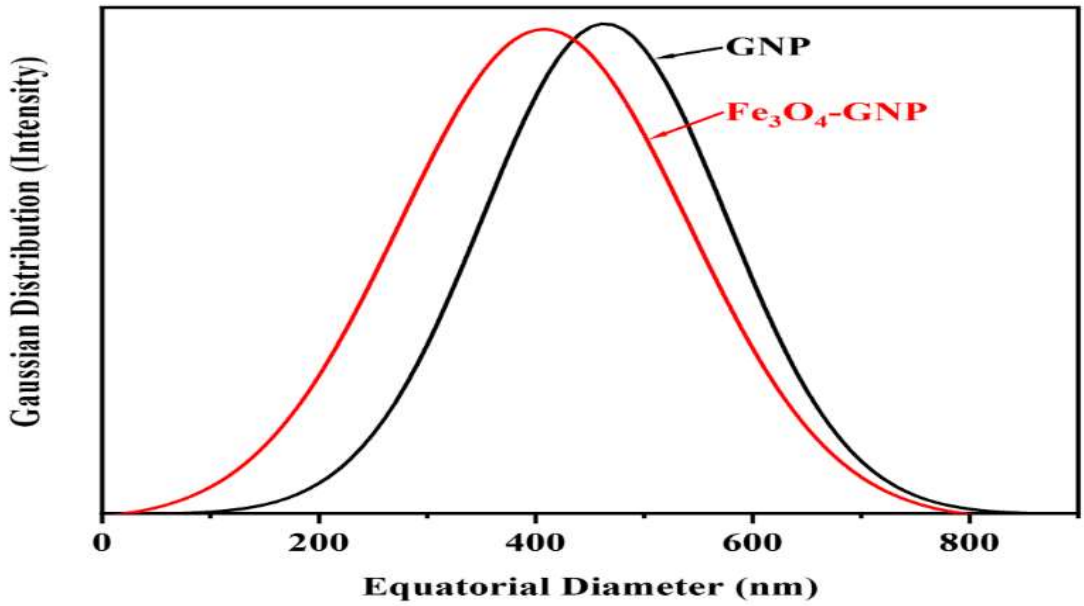

Fig. 4.15. Shows the Gaussian distribution of equatorial diameter of the GNP and Fe_3O_4-GNP measured by Dynamic light scattering.

Table 4.1. Roughness parameters of fractured surfaces for nanocomposites

Nanocomposite	Roughness parameters					
	R_a(nm)	% Increase	R_q(nm)	% Increase	R_z(nm)	% Increase
Neat epoxy	4.776	-	6.087	-	24.860	-
GNP epoxy	5.711	19.58	7.087	16.43	32.018	22.36
Fe_3O_4-GNP epoxy	7.959	66.65	10.352	70.01	48.810	96.34

4.4.11. Magnetic properties of GNP, Fe_3O_4, and Fe_3O_4-GNP

The magnetic hysteresis of the nanoparticles was measured at ambient temperature in a magnetic field that was applied and swept from -1T to 1T. **Fig. 3.8** depicts the Magnetic properties of GNP, Fe_3O_4 and Fe_3O_4-GNP. The details of the magnetic properties of the nanoparticles are summarised in **Table 4.2**. Tiny remanence and coercivity were present in the magnetic hysteresis of Fe_3O_4-GNP, indicating soft ferrimagnetic behaviour of it[194,195]. It appears that the Fe_3O_4-GNP has soft magnetic characteristics which were critical for magnetic alignment application. This improvement in GNP is a vital parameter for the alignment process.

Table 4.2.Magnetic properties of nanoparticles.

Nanoparticles	Magnetic properties at (300K, 40Hz)							
	M_s (emu/gm)	H_s (T)	M_r (emu/gm)	H_c (T)	Mass magnetic susceptibility (χ) (emu/gm-T)			
					$\overline{H}_0$=0.05 T	$\overline{H}_0$=0.1 T	$\overline{H}_0$=0.15 T	$\overline{H}_0$=0.2 T
GNP	~ 00	~ 00	~ 00	~ 00	~ 00	~ 00	~ 00	~ 00
Fe_3O_4	81	0.95	3.689	0.0049	536.11	223.48	84.06	38.20
Fe_3O_4-GNP	16	0.85	0.944	0.0044	76.81	20.27	8.53	6.49

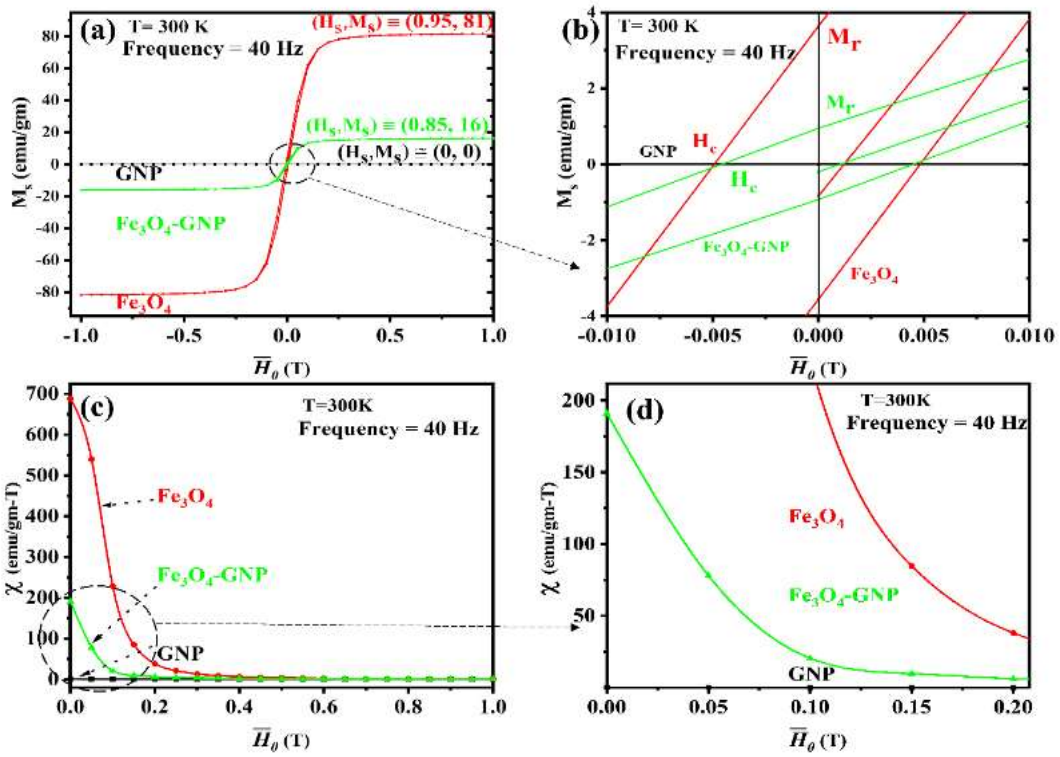

Fig. 4.16. Shows the (a) saturation magnetization (Ms) vs. applied Magnetic field ($\overline{H}_0$) having details the characteristics of coercivity and remanence, while (b) demonstrates the mass magnetic susceptibility(χ) vs. applied magnetic field ($\overline{H}_0$) of Fe_3O_4-GNP.

4.4.12. Chemorheological behaviour of epoxy during curing

Fig. 3.7 illustrates the chemorheological curve of the used reactive system during an isothermal test at 30^0 C. The viscous nature of the epoxy resin and hardener mixture can be observed over time. The viscosity of the reactive system increases with time. Still, the initial increase in the viscosity of epoxy is very gradual up to 15 minutes, after which the increment of the viscosity of these increases exponentially. It is clear that the viscosity of the epoxy rapidly increases after 30 minutes. After that, a gelation process prevents the solution from flowing. Finally, it can be concluded that the ideal casting time is ranged from 15 to 30 minutes.

In the second part of this paper, the characterization of Fe_3O_4, GNP, and Fe_3O_4-GNP is accomplished by HR-XRD, FTIR, Raman spectroscopy, TGA, BET, SEM, TEM, AFM, XPS, and VSM. The VSM study demonstrates that Fe_3O_4-GNP exhibits superparamagnetic behaviour due to Fe_3O_4 attachments to the GNP surfaces. The experimental setup based on our proposed model results is employed to align the Fe_3O_4-GNP nanoparticles in the liquid epoxy before epoxy gelation. The alignment of the nanoparticles in the epoxy are validated using XRD, SEM, Raman spectroscopy, and optical microscopy. The experimental characterization data are in good agreement with our model results. These results demonstrate that a highly oriented Fe_3O_4-GNP solution in the epoxy resin is produced in just a few minutes as well, as it was found that when employing an applied DC magnetic field, the field only needed to be applied when the system was getting close to the gel point rather than throughout the whole curing process. Finally, by attaching the magnetite nanoparticles (Fe_3O_4) to the surfaces of GNP, the non-covalent bonding of Fe_3O_4 nanoparticles to GNP surfaces allowed for the successful fabrication of the Fe_3O_4-GNP nanoparticles. We produced suitably dispersed and aligned Fe_3O_4-GNP nanocomposites. The nanocomposites are crucial for many applications, including structural, functional, biomedical, membrane, sense as many more.

4.5.Conclusion

This study provides a novel mathematical model [163] integrated experimental procedure to fabricate highly aligned Fe_3O_4-GNP epoxy nanocomposite with significant improvement in the functional material characterization to serve as a guideline for future generation advanced nanocomposite base structures. A highly aligned Fe_3O_4-GNP nanocomposite was fabricated employing our physical model of the alignment process induced by a moderately applied DC magnetic field.

This page intentionally left blank